

## **SURFACE TEMPERATURE IMPACT ON THE AERODYNAMIC SURFACE QUANTITIES OF HYPERSONIC GAP FLOW**

**Luis T. L. C. Paolicchi, [lucchi@lcp.inpe.br](mailto:lucchi@lcp.inpe.br)**  
**Wilson F. N. Santos, [wilson@lcp.inpe.br](mailto:wilson@lcp.inpe.br)**

Combustion and Propulsion Laboratory, National Institute for Space Research, Cachoeira Paulista, SP 12630-000

**Abstract** Numerical simulations of two-dimensional steady-state hypersonic flow in a gap at different length-to-depth ( $L/H$ ) ratio and wall temperature are performed by using a Direct Simulation Monte Carlo (DSMC) method. The  $L/H$  ratio varies from 1 to 1/4 and wall temperature ranges from 2 to 6 times the freestream temperature. The work focuses on the effects in the aerodynamic surface quantities, such as heat transfer, pressure and skin friction coefficients due to variations in the gap  $L/H$  ratio as well as in the wall temperature. It was found that the aerodynamic surface quantities presented a large dependence on the  $L/H$  ratio, and a small dependence on the wall temperature for the range investigated. The analysis showed that heat transfer, pressure, and skin friction coefficients presented the maximum values along the gap downstream face, more precisely, at the shoulder of the gap. Furthermore, the simulations showed that pressure and heating loads are several times larger than those for a smooth surface.

**Keywords:** DSMC, rarefied flow, hypersonic flow, gap, aerodynamic heating.

### **1. INTRODUCTION**

Separated and reattached supersonic flows have been under extensive interest in the last decades. These type of flows are frequent on surfaces of high-speed aerodynamic configurations, in which the performance is degraded by separated flows, and various components damaged due to intense heating loads at reattachment. Included in these flows are shock-boundary layer interactions, wakes, steps, cavity flows and gap flows. For instance, the thermal protection systems of vehicles like the space shuttle orbiter or crew rescue vehicle X-38 require gaps between the used protection elements to account for thermal expansion. For the optimized design of gaps and protection elements, it is necessary to predict the flow conditions and thermal loads as accurate as possible. In the case of reentry vehicles, the boundary layer transition prediction is a requirement to define the thermal protection system. This protection is usually designed as an assembly of tiles. The gaps between the tiles may modify the boundary layer state and eventually promote transition, inducing higher temperature levels than expected. Moreover, the gap flow structure can become even more complex if the gap dimensions are deformed by thermal or mechanical loads.

There is nowadays a rather extensive literature – mostly, but not entirely, experimental – dealing with the aerodynamic characteristics of gaps (Bertin and Goodrich, 1980; Everhart *et al.*, 2006; Hinderks *et al.*, 2004; Hinderks and Radespiel, 2006; Paolicchi and Santos, 2009; Petley *et al.*, 1984; Pitts and Murbach, 1982; Scott and Maraia, 1979; Smith *et al.*, 1983; Vharbonnier and Boerrigter, 1993). The majority of these research studies on gaps has gone into considering laminar or turbulent flow over a wide range of Mach numbers in the continuum flow regime. Usually, in the continuum flow regime, the gap flow topology is defined by the development of a column of counter-rotating vortices within the gap caused by the main stream flow, where the number of vortices is approximately given by  $H/L$ . Nevertheless, there is little understanding of the physical aspects of hypersonic flow past to gaps related to the severe aerothermodynamic environment associated to a reentry vehicle.

In this fashion, Paolicchi and Santos (2009) have studied gaps situated in a rarefied hypersonic flow by employing the DSMC method. The work was motivated by the interest in investigating the length-to-depth ( $L/H$ ) ratio effects on the flowfield structure. The primary emphasis was to examine the sensitivity of the velocity, density, pressure and temperature due to variations on the gap  $L/H$  ratio. The analysis showed that the recirculation region inside the gaps is a function of the  $L/H$  ratio. It was found only one vortex for the  $L/H$  ratio investigated. The results showed that gap flow behavior in the transition flow regime differs from that found in the continuum flow regime.

Having a clear qualitative picture of the flowfield structure in a gap, the present account extends further the previous analysis (Paolicchi and Santos, 2009) by investigating the impact of the wall temperature on the aerodynamic surface quantities. In this context, the primary goal of this paper is to assess the sensitivity of the heat transfer, pressure, and

skin friction coefficients to variations on the wall temperature for a family of gaps defined by different  $L/H$  ratio. The focus of the present study is the low-density region in the upper atmosphere. At this condition, the degree of molecular non-equilibrium is such that the Navier-Stokes equations are inappropriate. In such a circumstance, the Direct Simulation Monte Carlo (DSMC) method will be employed to calculate the hypersonic two-dimensional flow over the gaps.

## 2. GEOMETRY DEFINITION

Discontinuities or defects in a reentry capsule surface is modeled in the present work by a gap, length  $L$  and depth  $H$ , as defined in the previous work, Paolicchi and Santos (2009). By considering that the depth  $H$  is much smaller than the nose radius  $R$  of a reentry capsule, i.e.,  $H/R \ll 1$ , then the hypersonic flow over the gap may be considered as a hypersonic flow over a flat plate with a gap. Figure (1a) illustrates a schematic view of the model employed.

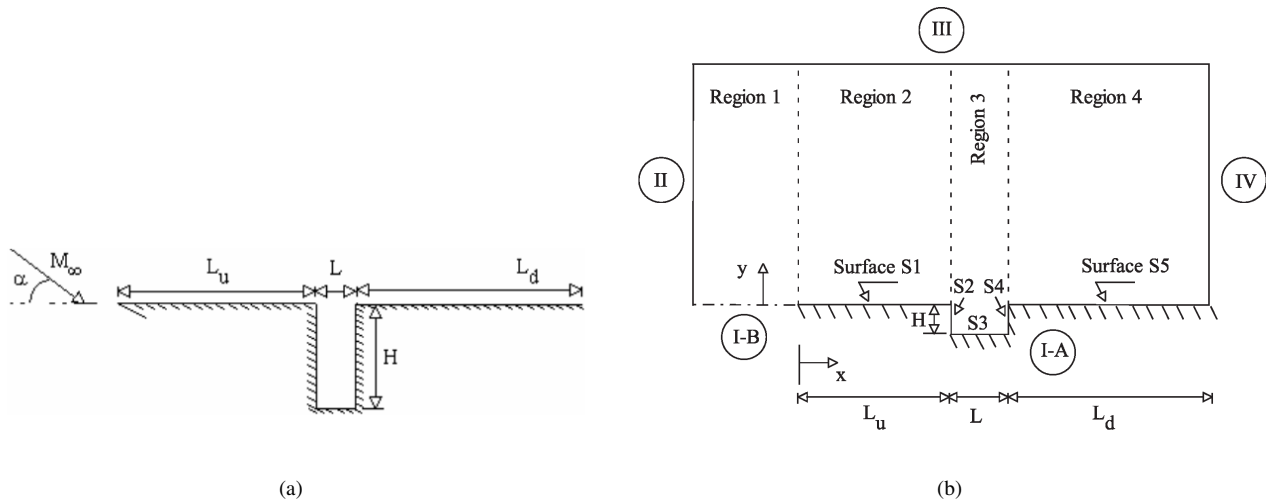


Figure 1. Drawing illustrating (a) a schematic view of the gap configuration and (b) the computational domain.

Referring to Fig. (1a),  $\alpha$  stands for the angle of attack,  $M_\infty$  represents the freestream Mach number,  $H$  the gap depth,  $L$  the gap length,  $L_u$  the length of the gap upstream surface, and  $L_d$  the length of the gap downstream surface. It was assumed a length  $L$  of 0.003 m, and a depth  $H$  of 0.003, 0.006, 0.009, and 0.012 m. Therefore, the gaps investigated correspond to a length-to-depth ratio,  $L/H$ , of 1, 1/2, 1/3 and 1/4, respectively. In addition,  $L_u/\lambda_\infty$  of 50 and  $L_d/\lambda_\infty$  of 50, where  $\lambda_\infty$  is the freestream mean free path. It was considered that the flat plate is infinitely long but only the total length  $L_u + L + L_d$  is investigated.

## 3. COMPUTATIONAL TOOL

The degree of departure of a flow from the continuum is indicated by the flow Knudsen number,  $Kn = \lambda/l$ , where  $\lambda$  is the molecular mean free path and  $l$  is a characteristic length of the flow. Traditionally, flows are divided into four regimes (Schaff and Chambre, 1958):  $Kn < 0.01$ , continuum flow,  $0.01 < Kn < 0.1$ , slip flow,  $0.1 < Kn < 10$ , transition flow, and  $Kn > 10$ , free molecular flow.

Flow in the regime of intermediate Knudsen numbers,  $0.01 < Kn < 10$ , is difficult to deal with analytically. Nowadays, the most successful numerical technique for modeling complex transition flows has been the Direct Simulation Monte Carlo (DSMC) method, introduced by Bird (1994). The DSMC method simulates real gas flows with various physical processes by means of a huge number of modeling particles, each of which is a typical representative of a great number of real gas molecules. DSMC models the flow as being a collection of discrete particles, each one with a position, velocity and internal energy. The state of the particles is stored and modified with time as the particles move, collide, and undergo boundary interactions in simulated physical space. The intermolecular collisions are uncoupled to the translational molecular motion over the time step used to advance the simulation. Time is advanced in discrete steps such that each step is small in comparison with the mean collision time (Garcia and Wagner, 2000; Hadjiconstantinou, 2000). The simulation is always calculated as unsteady flow. However, a steady flow solution is obtained as the large time state of the simulation.

The molecular collisions are modeled using the variable hard sphere (VHS) molecular model (Bird, 1981) and the no time counter (NTC) collision sampling technique (Bird, 1989). The VHS model assumes that the cross section of a molecule changes with the collision energy according to some power law. The exponent is calculated by matching the viscosity of the simulated gas to that of its real counterpart. In addition, the VHS model assumes an isotropic scattering

in the center of mass frame of reference.

Simulations are performed using a non-reacting gas model consisting of two chemical species,  $N_2$  and  $O_2$ . For polyatomic particles, transfer of energy to and from the internal modes has to be considered. In this way, energy exchanges between the translational and internal modes are considered. The energy exchange between kinetic and internal modes is controlled by the Borgnakke-Larsen statistical model (Borgnakke and Larsen, 1975). For a given collision, the probabilities are designated by the inverse of the relaxation numbers, which correspond to the number of collisions necessary, on average, for a molecule to relax. In this study, the relaxation numbers of 5 and 50 were used for the rotation and vibration, respectively.

#### 4. COMPUTATIONAL FLOW DOMAIN AND GRID

For the numerical treatment of the problem, the flowfield around the gap is divided into four regions, which are subdivided into computational cells. The cells are further subdivided into subcells, two subcells/cell in each coordinate direction. The cell provides a convenient reference for the sampling of the macroscopic gas properties, while the collision partners are selected from the same subcell for the establishment of the collision rate. The dimensions of the cells must be such that the change in flow properties across each cell is small. The linear dimensions of the cells should be small in comparison with the scale length of the macroscopic flow gradients normal to streamwise directions, which means that the cell dimensions should be the order of or even smaller than the local mean free path (Alexander *et al.*, 1998, 2000).

The computational domain used for the calculation is made large enough so that gap disturbances do not reach the upstream and side boundaries, where freestream conditions are specified. A schematic view of the computational domain is illustrated in Fig. (1b). According to this figure, side I-A is defined by the gap surface. Diffuse reflection with complete thermal accommodation is the condition applied to this side. Side I-B is a plane of symmetry, where all flow gradients normal to the plane are zero. At the molecular level, this plane is equivalent to a specular reflecting boundary. Sides II and III are the freestream side through which simulated molecules enter and exit. Side II is positioned at  $5\lambda_\infty$  upstream of the flat-plate leading edge, and side III defined at  $25\lambda_\infty$  above the flat plate. Finally, the flow at the downstream outflow boundary, side IV, is predominantly supersonic and vacuum condition is specified (Bird, 1994). At this boundary, simulated molecules can only exit.

Numerical accuracy in DSMC method depends on the grid resolution chosen as well as on the number of particles per computational cell. Both effects were investigated to determine the number of cells and the number of particles required to achieve grid independence solutions. A grid independence study was made with three different structured meshes – coarse, standard and fine – in each coordinate direction. The effect of altering the cell size in the  $x$ -direction was investigated for a coarse and fine grids with, respectively, 50% less and 100% more cells with respect to the standard grid only in the  $x$ -direction. Table (1) tabulates the number of cells employed in the four regions for coarse, standard, and fine grids for the  $L/H = 1$  case.

In analogous fashion, an examination was made in the  $y$ -direction with a coarse and fine grids with, respectively, 50% less and 100% more cells with respect to the standard grid only in the  $y$ -direction. In addition, each grid was made up of non-uniform cell spacing in both directions. Moreover, point clustering is used close to solid walls and to the horizontal plane connecting the two corners. The effect (not shown) of changing the cell size in both directions on the heat transfer, pressure and skin friction coefficients was rather insensitive to the range of cell spacing considered, indicating that the standard grid, with a total of 15,000 cells, for the  $L/H = 1$  case, is essentially grid independent.

A similar examination was made for the number of molecules. The standard grid for the  $L/H = 1$  case corresponds to, on average, a total of 314,700 molecules. Two new cases using the same grid were investigated. These two new cases correspond to 157,500 and 630,600 molecules in the entire computational domain. As the three cases presented the same results (not shown) for the heat transfer, pressure and skin friction coefficients, hence the standard grid with a total of 314,700 molecules is considered enough for the computation of the flowfield properties.

Table 1. Number of cells in the ( $x$ -direction investigation) and [ $y$ -direction investigation] for the  $L/H = 1$  case.

	Region 1	Region 2	Region 3	Region 4	Total number of cells
<b>Coarse</b>	( 5 × 40)	( 60 × 50)	(10 × 70)	( 60 × 60)	7,500
	[10 × 20]	[120 × 25]	[20 × 35]	[120 × 30]	30,000
<b>Standard</b>	10 × 40	120 × 50	20 × 70	120 × 60	15,000
<b>Fine</b>	(20 × 40)	(240 × 50)	(40 × 70)	(240 × 60)	7,500
	[10 × 80]	[120 × 100]	[20 × 140]	[120 × 120]	30,000

## 5. FREESTREAM AND FLOW CONDITIONS

Freestream and flow conditions represent those experienced by a capsule at an altitude of 70 km. In the present account, freestream flow conditions used for the numerical simulations are those given by Paolicchi and Santos (2009) and summarized in Tab. (2), and the gas properties (Bird, 1994) are shown in Tab. (3).

Table 2. Freestream flow conditions

Altitude (km)	$T_\infty$ (K)	$p_\infty$ (N/m <sup>2</sup> )	$\rho_\infty$ (kg/m <sup>3</sup> )	$n_\infty$ (m <sup>-3</sup> )	$\lambda_\infty$ (m)	$U_\infty$ (m/s)
70	219.07	5.518	$8.752 \times 10^{-5}$	$1.8193 \times 10^{21}$	$9.285 \times 10^{-4}$	7456

Table 3. Gas properties

$X$	$m$ (kg)	$d$ (m)	$\omega$	
$O_2$	0.237	$5.312 \times 10^{-26}$	$4.01 \times 10^{-10}$	0.77
$N_2$	0.763	$4.650 \times 10^{-26}$	$4.11 \times 10^{-10}$	0.74

The freestream velocity  $U_\infty$  is assumed to be constant at 7456 m/s, which corresponds to a freestream Mach number  $M_\infty$  of 25. The translational and vibrational temperatures in the freestream are in equilibrium at 219.07 K. In order to simulate the gap surface temperature effects, the wall temperature  $T_w$  is assumed constant at 440 K, 880 K, and 1320 K, which correspond approximately to 2, 4, and 6 times the freestream temperature  $T_\infty$ . In addition, a flow with zero-degree angle of attack was assumed in this investigation.

By assuming the gap depth  $H$  as the characteristic length, the Knudsen number  $Kn_H$  corresponds to 0.3095, 0.1548, 0.1032, and 0.0774 for depth  $H$  of 0.003, 0.006, 0.009, and 0.012 m, respectively. Finally, the Reynolds number  $Re_H$  is around 121.7, 243.4, 365.1, and 486.8 for depth  $H$  of 0.003, 0.006, 0.009, and 0.012 m, respectively, also based on conditions in the undisturbed stream.

## 6. COMPUTATIONAL RESULTS AND DISCUSSION

This section concentrates on the effects that take place in the aerodynamic surface quantities due to wall temperature variations. Aerodynamic surface quantities of particular interest in the transitional flow regime are number flux, pressure, heat transfer, and skin friction. In this scenario, the purpose of this section is to present and to discuss changes on these quantities, expressed in coefficient form, due to variations on the wall temperature as well as on the gap  $L/H$  ratio.

### 6.1 Number Flux

As the wall temperature  $T_w$  is increased from 440 K to 1320 K, the molecules impinging on the gap surface are reflected with greater energies. The relative translational velocities of reflected molecules close to the surface will be increased, thus reducing the net buildup of particle density near the body surface. As a result, changes in the number of molecules colliding with the surface as well as changes in the incident or reflected momentum and energy of these molecules are expected.

The number flux  $N$  is calculated by sampling the molecules impinging on the surface by unit time and unit area. The sensitivity of the number flux to variations on the  $L/H$  ratio for the  $T_w = 440$  K case is illustrated in Figs. 2(a-c) for gap surfaces  $S_2$ ,  $S_3$  and  $S_4$ , respectively. In a similar way, Figs. 3(a-c) demonstrate the number flux distribution for the  $T_w = 1320$  K case along the gap surfaces  $S_2$ ,  $S_3$  and  $S_4$ , respectively. In this group of plots,  $N_f$  represents the number flux  $N$  normalized by  $n_\infty U_\infty$ , where  $n_\infty$  is the freestream number density and  $U_\infty$  is the freestream velocity. In addition, the dimension height  $Y'$  is the height  $y$  normalized by the gap height  $H$ , and  $X'$  represents the distance  $(x - L_u)$  normalized by the gap length  $L$ . Also,  $S_2$ ,  $S_3$  and  $S_4$  stand for the gap vertical surfaces, *i.e.*, upstream and downstream faces, and horizontal gap surface, *i.e.*, the gap floor or the bottom surface, as defined in Fig. (1b). It is important to mention that results for the  $T_w = 880$  K case are intermediate to those for 440 K and 1320 K cases and, therefore, they will not be shown.

According to Figs. 2(a-c), it is seen that the dimensionless number flux  $N_f$  to the surface relies on the  $L/H$  ratio. For the upstream face, surface  $S_2$ , the dimensionless number flux is low at the top of the gap, and increases gradually along the surface up to the corner at the bottom surface. In contrast, for the downstream face, surface  $S_4$ , the dimensionless number

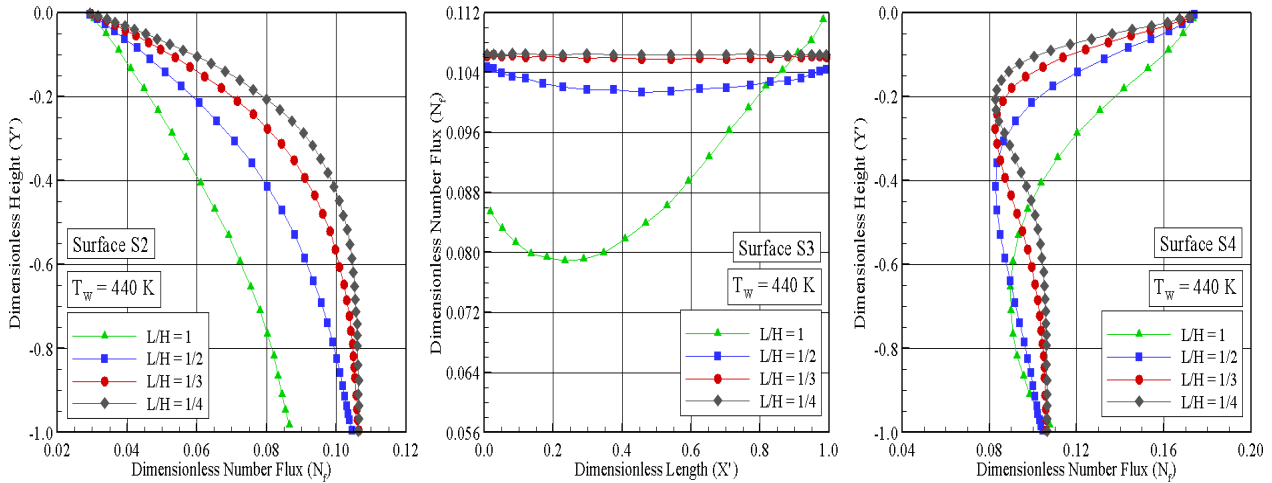


Figure 2. Dimensionless number flux ( $N_f$ ) distribution along the gap surface (a)  $S_2$ , (b)  $S_3$ , and (c)  $S_4$  for the  $T_w = 440$  K case.

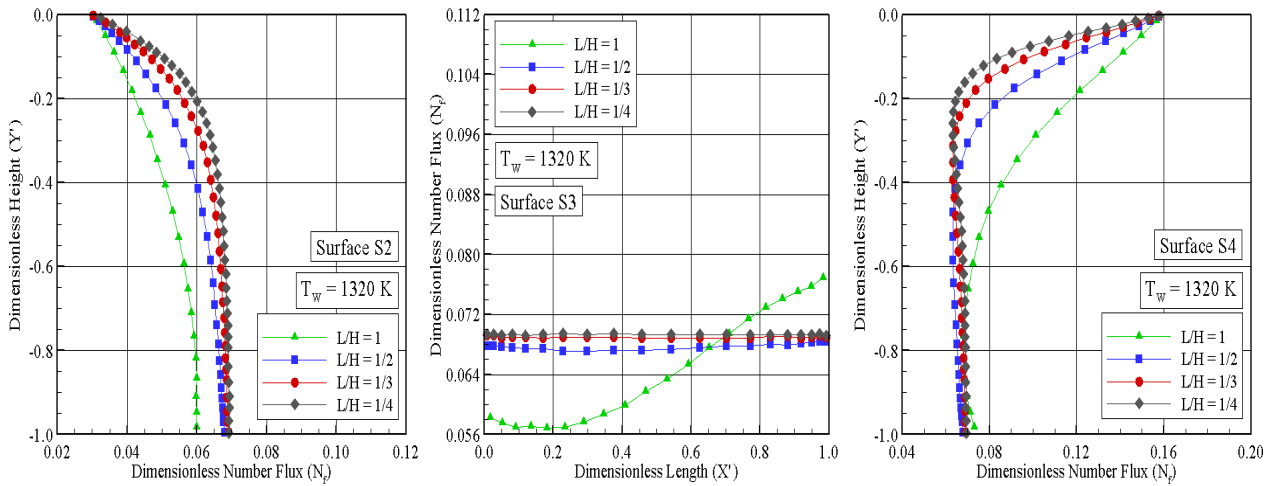


Figure 3. Dimensionless number flux ( $N_f$ ) distribution along the gap surface (a)  $S_2$ , (b)  $S_3$ , and (c)  $S_4$  for the  $T_w = 1320$  K case.

flux is high at the top of the gap, and decreases gradually to a minimum value, which is a function of the  $L/H$  ratio. After that, it slightly increases along the surface up to the corner at the bottom surface. Along the gap floor, surface  $S_3$ , the dimensionless number flux behavior also depends on  $L/H$  ratio. It basically presents a constant value with increasing the  $L/H$  ratio.

Referring to Figs. 2 and 3, it is observed that the number flux relies not only on the  $L/H$  ratio but also on the wall temperature. As the wall temperature is increased from 440 K to 1320 K, a reduction on the number flux to the surfaces  $S_2$ ,  $S_3$  and  $S_4$  is clearly seen. This is an expected behavior in the sense that, with increasing the body surface temperature, the molecules are reflected from the surface with greater energies. Consequently, the net buildup of particle density near the body surface is reduced.

Particular attention is paid to the maximum value for the dimensionless number flux. Based on Figs. 2 and 3, the maximum values for  $N_f$ , taking place at the gap shoulder, at the  $S_4/S_5$  surface junction, are approximately of 0.174, 0.163 (not shown), and 0.158 for wall temperature of 440 K, 880 K, and 1320 K, respectively. For comparative purpose, according to Leite and Santos (2009), the peak value for  $N_f$  in a flat plate, which corresponds to a smooth surface as compared to a flat plate with a gap, is around 0.07, in a station corresponding to  $26.5\lambda_\infty$  from the leading edge, for the same freestream flow conditions and wall temperature of 880 K.

## 6.2 Heat Transfer Coefficient

The heat transfer coefficient  $C_h$  is defined as follows,

$$C_h = \frac{q_w}{\frac{1}{2}\rho_\infty U_\infty^3} \quad (1)$$

where the heat flux  $q_w$  to the body surface is calculated by the net energy flux of the molecules impinging on the surface. A flux is regarded as positive if it is directed toward the body surface. The net heat flux  $q_w$  is related to the sum of the translational, rotational and vibrational energies of both incident and reflected molecules as defined by,

$$q_w = q_i - q_r = \sum_{j=1}^N \left[ \frac{1}{2} m_j c_j^2 + e_{Rj} + e_{Vj} \right]_i - \sum_{j=1}^N \left[ \frac{1}{2} m_j c_j^2 + e_{Rj} + e_{Vj} \right]_r \quad (2)$$

where  $N$  is the number of molecules colliding with the surface by unit time and unit area,  $m$  is the mass of the molecules,  $c$  is the velocity of the molecules,  $e_R$  and  $e_V$  stand for the rotational and vibrational energies, respectively. Subscripts  $i$  and  $r$  refer to incident and reflect molecules.

The dependence of the heat transfer coefficient  $C_h$  on the  $L/H$  ratio is demonstrated in Figs. (4) and (5) for wall temperature of 440 K and 1320 K, respectively. It is noticed from this set of diagrams that the heat transfer coefficient  $C_h$  is sensitive to the  $L/H$  ratio. Nevertheless, no appreciable change is observed in the heat transfer coefficient with the wall temperature rise for the temperature range investigated. For the upstream face, surface  $S2$ , the heat transfer coefficient is high at the top of the gap, and increases to a maximum value close to the top. Afterwards, it drops off along the surface up to the corner at the bottom surface. Along the gap floor, surface  $S3$ , the heat transfer coefficient depends on the  $L/H$  ratio.  $C_h$  basically decreases to zero by increasing the  $L/H$  ratio. For the downstream face, surface  $S4$ , the heat transfer coefficient is high at the top of the gap, and dramatically decreases along the surface, reaching  $C_h = 0$  at the corner. It is also very encouraging to observe that the heat transfer coefficient  $C_h$  for the downstream face is roughly one order of magnitude larger than that for the bottom surface, and this is one order of magnitude larger than that for the upstream face. One possible reason for that is because at the vicinity of the upstream face the flow experiences an expansion. In contrast, at the vicinity of the downstream face, it experiences a compression due to the recirculation inside the gap (Paolicchi and Santos, 2009).

The heat flux to the body surface was defined in terms of the incident and reflected flow properties, Eq.( 2), and based upon the gas-surface interaction model of fully accommodated, complete diffuse re-emission. The diffuse model assumes that the molecules are reflected equally in all directions, quite independently of their incident speed and direction. Due to the diffuse reflection model, the reflected velocity of the molecules impinging on the body surface is obtained from a Maxwellian distribution that takes into account for the temperature of the body surface. In this fashion, according to Eq.( 2), not only the number of molecules impinging on the surface but also the wall temperature plays an important role on the reflected contribution to the net heat flux to the body surface.

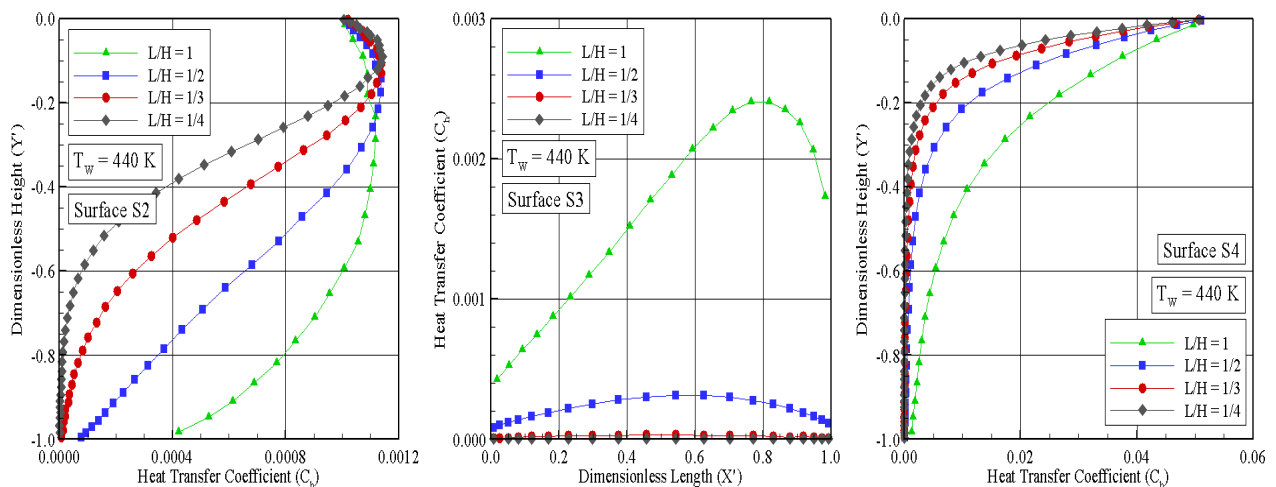


Figure 4. Heat transfer coefficient ( $C_h$ ) distribution along the gap surface (a)  $S2$ , (b)  $S3$ , and (c)  $S4$  for the  $T_w = 440$  K case.

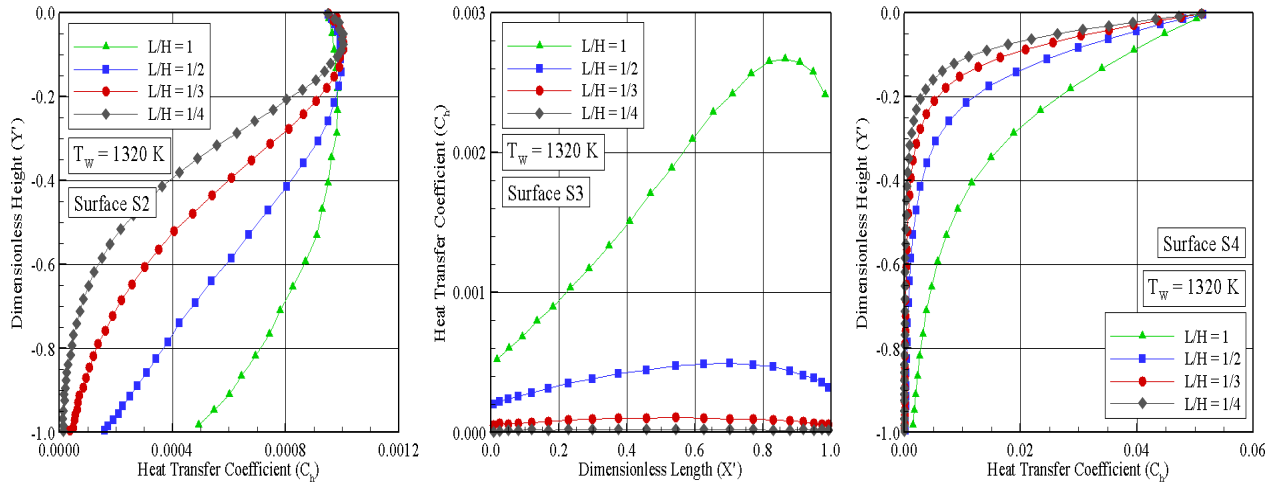


Figure 5. Heat transfer coefficient ( $C_h$ ) distribution along the gap surface (a)  $S_2$ , (b)  $S_3$ , and (c)  $S_4$  for the  $T_w = 1320$  K case.

Of particular interest is the behavior of the heat transfer coefficient  $C_h$  at the vicinity of the gap shoulder in the upstream face, surface  $S_2$ , Figs. (4a) and (5a). It is clearly noticed that the  $C_h$  reaches the peak value around the station  $Y' = 0.1$ . As the number of molecules impinging on the gap surface at the vicinity of this station is low, as shown by Figs. (2a) and (3a), then the velocity of the molecules increases in this region in order to increase the heat transfer coefficient in this region. As a matter of fact, a molecular velocity rise in this region is expected due to the flow expansion along the shoulder of the gap, *i.e.*, the  $S_1/S_2$  surface junction.

At this point it is worth taking a closer look at these results. In order to do that, the peak values for the heat transfer coefficient,  $C_h \approx 0.051$  at the gap shoulder for wall temperature  $T_w$  of 440 K, 880 K, and 1320 K, are compared to that predicted for a smooth surface, *i.e.*, a flat plate without a gap. According to Leite and Santos (2009), for the same freestream conditions and wall temperature of 880 K, the maximum value for  $C_h$  is around to 0.029 at a station  $8.4\lambda_\infty$  from the leading edge. Therefore, the peak value of  $C_h$  for the gap is approximately twice of that for a smooth surface.

### 6.3 Pressure Coefficient

The pressure coefficient  $C_p$  is defined as follows,

$$C_p = \frac{p_w - p_\infty}{\frac{1}{2}\rho_\infty U_\infty^2} \quad (3)$$

where the pressure  $p_w$  on the body surface is calculated by the sum of the normal momentum fluxes of both incident and reflected molecules at each time step as follows,

$$p_w = p_i - p_r = \sum_{j=1}^N \{[(mv)_j]_i - [(mv)_j]_r\} \quad (4)$$

where  $v$  is the velocity component of the molecule  $j$  in the surface normal direction.

The effect on pressure coefficient  $C_p$  due to variations on the  $L/H$  ratio is demonstrated in Figs. (6) and (7) for wall temperature of 440 K and 1320 K, respectively.

Looking first to Figs. (6a-c), it is seen that the pressure coefficient  $C_p$  roughly follows the same trend as that presented by the number flux in the sense that, for the upstream face, surface  $S_2$ , it presents the lower value at the shoulder,  $Y' = 0$ , increases along the upper half part of the surface, and basically reaches a constant value along the lower half part of the surface. In the following, for the gap floor, surface  $S_3$ , the pressure coefficient presents the same behavior for the  $L/H < 1$ , *i.e.*, a constant value along the entire surface. Finally, along the downstream face, surface  $S_4$ , the pressure coefficient behavior is in contrast to that observed along the surface  $S_2$  in the sense that  $C_p$  is constant along the lower half part of the surface and increases along the upper half part of the surface, reaching the peak value at the shoulder,  $Y' = 0$ . It may be inferred in passing that this is an expected behavior since the flow within the gap is characterized by the appearance of a clockwise recirculation region. According to Paolicchi and Santos (2009), the streamline pattern shows

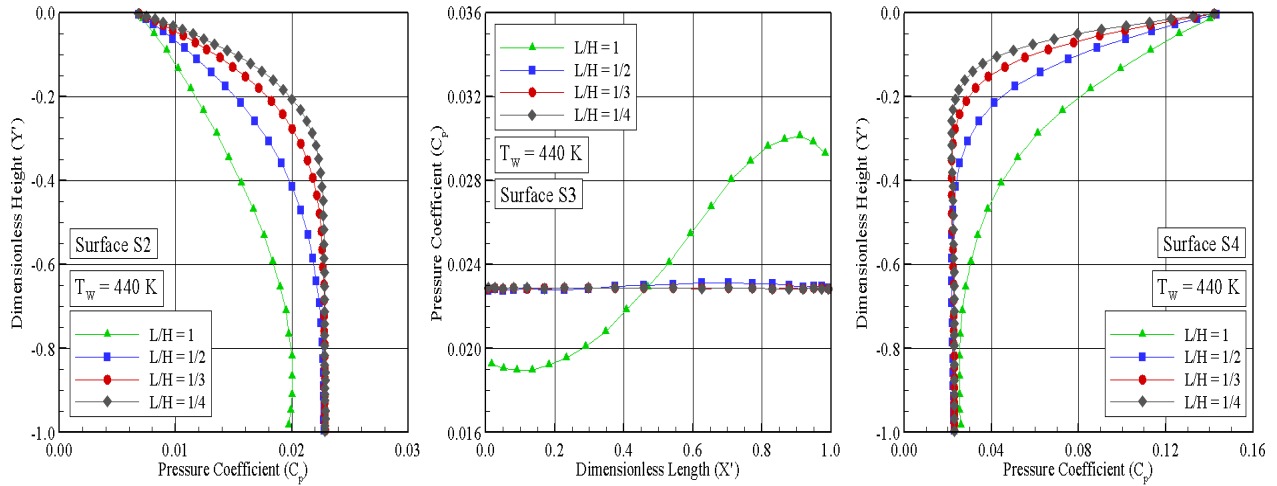


Figure 6. Pressure coefficient ( $C_p$ ) distribution along the gap surface (a)  $S_2$ , (b)  $S_3$ , and (c)  $S_4$  for the  $T_w = 440$  K case.

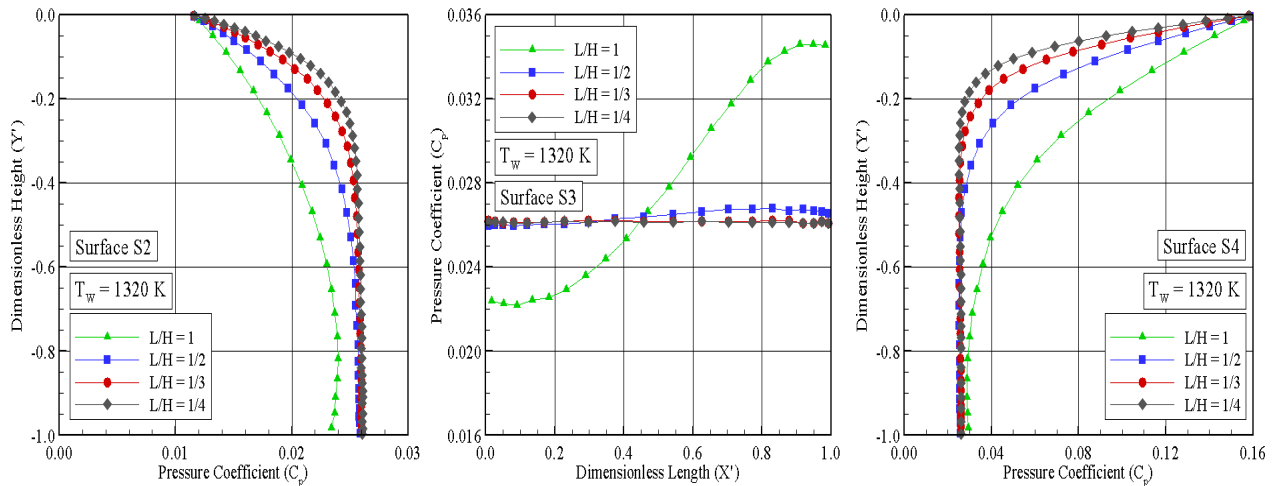


Figure 7. Pressure coefficient ( $C_p$ ) distribution along the gap surface (a)  $S_2$ , (b)  $S_3$ , and (c)  $S_4$  for the  $T_w = 1320$  K case.

that the flow is characterized by a primary vortex system. For the  $L/H = 1$  and  $1/2$  cases, the recirculating structure fills the entire gaps. Conversely, for the  $L/H = 1/3$  and  $1/4$  cases, the recirculating structure does not fill the entire gaps.

Turning next to Figs. (7a-c), it is found that the wall temperature rise has no expressive effect on the pressure coefficient  $C_p$  for the range investigated. It is seen that the pressure coefficient slightly increases along the surfaces  $S_2$ ,  $S_3$  and  $S_4$ . It may be concluded from Eq. (3) that a pressure coefficient rise is associated to an increase in the wall pressure  $p_w$ . In addition, based on Eq. (4), a wall pressure rise is related to an increase in the number of molecules colliding to the surface and/or an increase in the velocity of the molecules. At this point, it is important to recognize from the number flux distribution, Figs. (2) and (3), that the number flux to the surfaces decreased with increasing the wall temperature. In addition, with increasing the wall temperature, the molecules are reflected with more energy. Therefore, there is an indication that the energetic scattered molecules play a more significant role, with the incident component of the wall pressure decreasing and the reflected one increasing with the wall temperature rise. Hence, the insensitivity of the pressure coefficient to wall temperature variations in the range investigated, shown in Figs. (7a-c), is primarily attributed to a counterbalance between the number flux reduction and the normal momentum rise related to the reflected molecules.

In what follows, it proves helpful to compare the maximum values for the pressure coefficient observed in the gaps with that of a smooth surface, *i.e.*, a flat plate without a gap. As a basis of comparison, the peak values for  $C_p$ , around 0.15, are observed at the gap shoulder, surface  $S_4$ . According to Leite and Santos (2009), for the same freestream conditions and wall temperature of 880 K, the maximum value for  $C_p$  is around 0.039 at a station  $24.2\lambda_\infty$  from the leading edge. Therefore, the peak value of  $C_p$  for the gap is around four times larger than that for a smooth surface.

## 6.4 Skin Friction Coefficient

The skin friction coefficient  $C_f$  is defined as follows,

$$C_f = \frac{\tau_w}{\frac{1}{2}\rho_\infty U_\infty^2} \quad (5)$$

where the shear stress  $\tau_w$  on the body surface is calculated by the sum of the tangential momentum fluxes of both incident and reflected molecules impinging on the surface at each time step by the following expression,

$$\tau_w = \tau_i - \tau_r = \sum_{j=1}^N \{[(mu)_j]_i - [(mu)_j]_r\} \quad (6)$$

where  $u$  is the velocity component of the molecule  $j$  in the surface tangential direction.

It is worthwhile to note that for the special case of diffuse reflection, the gas-surface interaction model adopted herein, the reflected molecules have a tangential moment equal to zero, since the molecules essentially lose, on average, their tangential velocity components. In this fashion, the tangential momentum flux of the incident molecules is defined as follows,

$$\tau_w = \tau_i = \sum_{j=1}^N \{[(mu)_j]_i\} \quad (7)$$

The effect of the  $L/H$  ratio on the skin friction coefficient  $C_f$  is depicted in Figs. (8) and (9) for wall temperature of 440 K and 1320 K, respectively. According to this set of plots, it is noticed that, for the upstream face, surface  $S_2$ , the skin friction coefficient in general presents the peak value at the shoulder,  $Y' = 0$ , decreases along the upper half part of the surface, and basically reaches a negative constant value along the lower half part of the surface. In what follows, for the gap floor, surface  $S_3$ , the skin friction coefficient is negative near the vicinity of the  $S_2/S_3$  surface junction, and becomes positive at the vicinity of the  $S_3/S_4$  surface junction. Nevertheless, as the  $L/H$  ratio increases, the condition  $C_f \approx 0$  is observed along the entire surface. Finally, along the downstream face, surface  $S_4$ , the skin friction coefficient starts from zero at the vicinity of the  $S_3/S_4$  surface junction and decreases negatively up to the minimum value at the shoulder,  $Y' = 0$ . Usually, as  $C_f$  changes from positive to negative value,  $C_f = 0$  may indicate the presence of a backflow, an attachment or reattachment point in the flow. In the present account, these changes are directly related to the clockwise recirculation region.

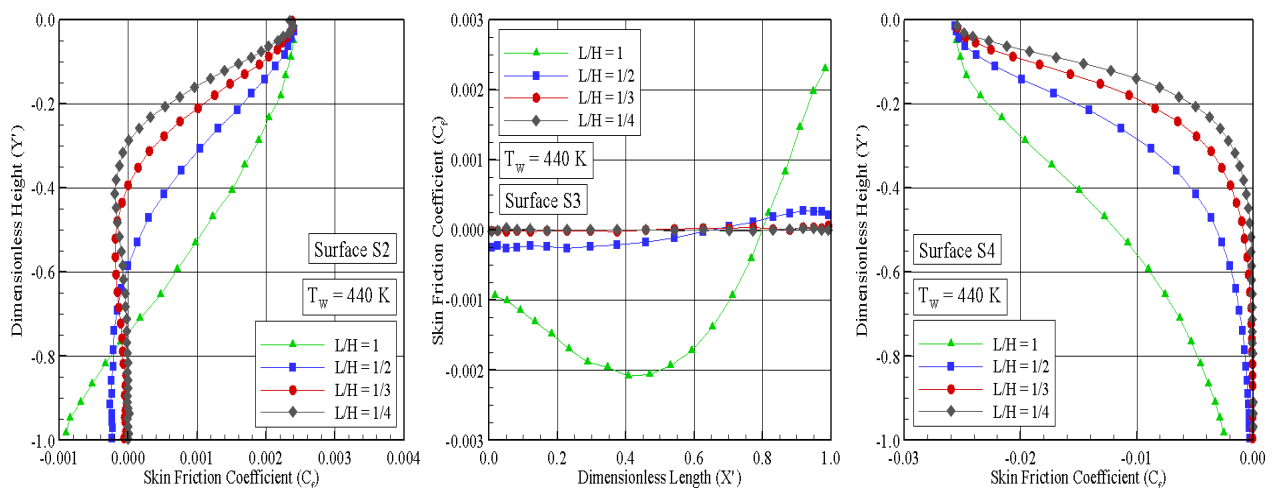


Figure 8. Skin friction coefficient ( $C_f$ ) distribution along the gap surface (a)  $S_2$ , (b)  $S_3$ , and (c)  $S_4$  for the  $T_w = 440$  K case.

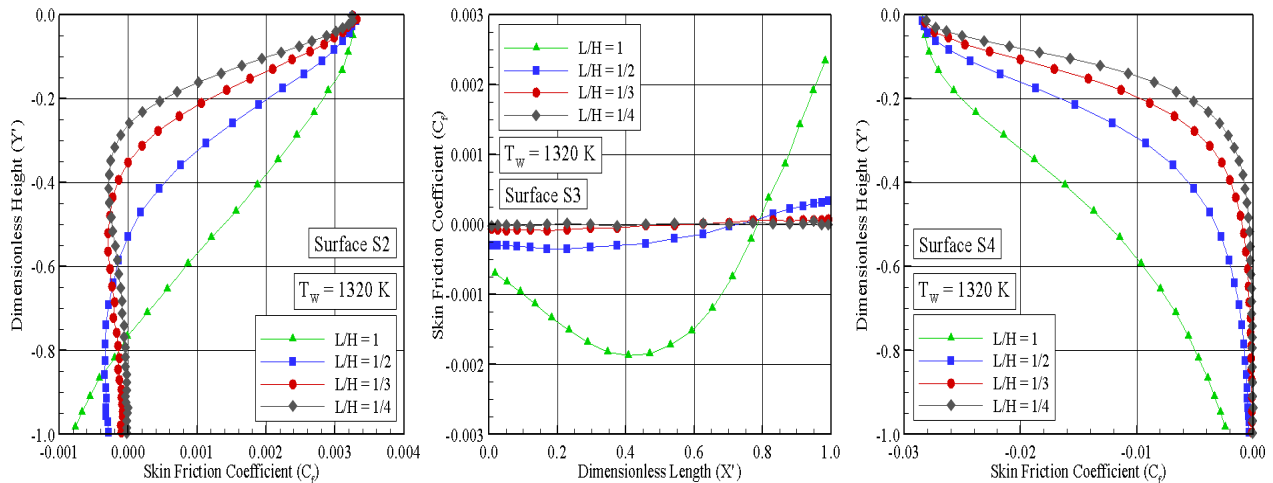


Figure 9. Skin friction coefficient ( $C_f$ ) distribution along the gap surface (a)  $S_2$ , (b)  $S_3$ , and (c)  $S_4$  for the  $T_w = 1320$  K case.

## 7. CONCLUDING REMARKS

Computations of a rarefied hypersonic flow on a family of gaps have been performed by using the Direct Simulation Monte Carlo (DSMC) method. The calculations provided information concerning the nature of the aerodynamic surface quantities on the gaps. Effects of the length-to-depth ratio and effects of the wall temperature on the number flux, heat transfer, pressure and skin friction coefficients for a representative range of parameters were investigated. The wall temperature varied from 440 K to 1320 K, and the length-to-depth ratio ranged from 1 to 1/4, which corresponded Knudsen numbers in the transitional flow regime.

On the basis of the foregoing results it was concluded that, for the range of the conditions of the present investigation, the aerodynamic quantities acting on the gap surface depend on the  $L/H$  ratio. In contrast, the aerodynamic surface quantities presented a small dependence on the wall temperature. It was found that the pressure load and the heat load presented the maximum values along the gap downstream face, more precisely, at the shoulder of the gap. In addition, these loads are much larger than those attained in a smooth surface.

## 8. ACKNOWLEDGMENT

The authors would like to thank the financial support provided by CNPq (Conselho Nacional de Desenvolvimento Científico e Tecnológico) under Grant No. 473267/2008-0.

## 9. REFERENCES

- Alexander, F. J., Garcia, A. L., and Alder, B. J., 1998. "Cell Size Dependence of Transport Coefficient in Stochastic Particle Algorithms", *Physics of Fluids*, Vol. 10, pp. 1540–1542.
- Alexander, F. J., Garcia, A. L., and Alder, B. J., 2000. "Erratum: Cell Size Dependence of Transport Coefficient in Stochastic Particle Algorithms", *Physics of Fluids*, Vol. 12, pp. 731–731.
- Bertin, J. J., and Goodrich, W. D., 1980. "Aerodynamic Heating for Gaps in Laminar and Transitional Boundary Layers", 18th AIAA Aerospace Sciences Meeting and Exhibit, AIAA Paper 80-0287, Pasadena, CA, USA, January 14–16.
- Bird, G. A., 1981. "Monte Carlo Simulation in an Engineering Context", In Fisher, S. S., ed., *Progress in Astronautics and Aeronautics: Rarefied Gas Dynamics*, Vol. 74, part I, AIAA New York, pp. 239–255.
- Bird, G. A., 1989. "Perception of Numerical Method in Rarefied Gasdynamics", In Muntz, E. P., Weaver, D. P., and Capbell, D. H., eds., *Rarefied Gas Dynamics: Theoretical and Computational Techniques*, Vol. 118, Progress in Astronautics and Aeronautics, AIAA, New York, pp. 374–395.
- Bird, G. A., 1994. *Molecular Gas Dynamics and the Direct Simulation of Gas Flows*, Oxford University Press.
- Borgnakke, C. and Larsen, P. S., 1975. "Statistical Collision Model for Monte Carlo Simulation of Polyatomic Gas Mixture", *Journal of Computational Physics*, Vol. 18, No. 4, pp. 405–420.
- Everhart, J. L., Alter, S. J., Merski, N. R., and Wood, W. A., 2006. "Pressure Gradient Effects on Hypersonic Cavity Flow Heating", 44th AIAA Aerospace Sciences Meeting and Exhibit, AIAA Paper 2006-0185, Reno, NV.
- Garcia, A. L., and Wagner, W., 2000. "Time Step Truncation Error in Direct Simulation Monte Carlo", *Physics of Fluids*,

Vol. 12, pp. 2621–2633.

- Hadjiconstantinou, N. G., 2000. “Analysis of Discretization in the Direct Simulation Monte Carlo”, *Physics of Fluids*, Vol. 12, pp. 2634–2638.
- Hinderks, M., Radespiel, R., and Gülhan, A., 2004. “Simulation of Hypersonic Gap Flow with Consideration of Fluid Structure Interaction”, 34th AIAA Fluid Dynamics Conference and Exhibit, AIAA Paper 2004–2238, Portland, OR.
- Hinderks, M. and Radespiel, R., 2006. “Investigation of Hypersonic Gap Flow of a Reentry Nosecap with Consideration of Fluid structure Interaction”, 44th AIAA Aerospace Sciences Meeting and Exhibit, AIAA Paper 2006-0188, Reno, NV, USA, January 9–12, 2006.
- Leite, P. H. M., and Santos, W. F. N., 2009. “Direct Simulation of Heat Transfer and Pressure Distributions of Hypersonic Flow over a Backward-Facing Steps”, XII Encontro de Modelagem Computacional, EMC 2009, December 2–4, Rio de Janeiro, RJ.
- Paolicchi, L. T. L. C., and Santos, W. F. N., 2009. “Direct Simulation Calculations of Rarefied Hypersonic Gap Flow”, 3rd Southern Conference on Computational Modeling, Rio Grande, RS, Nov. 23–25 Nov.
- Petley, D. H., Smith, D. M., Edwards, C. L. W., Carlson, A. B., and Hamilton II, H. H., 1984. “Surface Step Induced Gap Heating in the Shuttle Thermal Protection System”, *Journal of Spacecraft and Rockets*, vol. 11, no. 2, pp. 156–161.
- Pitts, W. C., and Murbach, M. S., 1982. “Flight Measurements of Tile Gap Heating on the Space Shuttle”, AIAA/ASME 3rd Joint Thermophysics, Fluids, Plasma and Heat Transfer Conference, AIAA Paper 82–0840, St. Louis, MO.
- Schaff, S. A. and Chambre P. L., 1958. *Fundamentals of Gas Dynamics*, Princeton University Press, Princeton, NJ.
- Scott, C. D., and Maraia, R. J., 1979. “Gap Heating with Pressure Gradients”, 14th AIAA Thermophysics Conference, AIAA Paper 79–1043, Orlando, FL, USA, June 4–6, 1979.
- Smith, D. M., Petley, D. N., Edwards, C. L. W., and Patten, A. B., 1983. “An Investigation of Gap Heating Due to Stepped Tiles in Zero Pressure Gradient Regions of the Shuttle Orbiter Thermal Protection System”, 21st AIAA Aerospace Sciences Meeting and Exhibit, AIAA Paper 83-0120, Reno, NV, USA, January 10–13.
- Vharbonnier, J., and Boerrigter, H., 1993. “Contribution to the Study of Gap Induced Boundary Layer Transition in Hypersonic Flow”, AIAA/DGLR 5th International Aerospace Planes and Hypersonics Technologies Conference, AIAA Paper 93–5111, Munich, Germany.

## 10. RESPONSIBILITY NOTICE

The authors are the only responsible for the printed material included in this paper.